

## 4.9 Report of Project Part 09: CAD of semiconductor nanodevices

### Computer-aided design of semiconductor nanodevices

**Principal investigator:**     **Hans Kosina**  
Technische Universität Wien  
Institut für Mikroelektronik  
Gußhausstraße 27-29, A-1040 Wien  
Phone: +43 1 58801 36013  
Fax: +43 1 58801 36099  
eMail: kosina@iue.tuwien.ac.at

#### 4.9.1 Summary

A numerical simulator for electron transport in quantum cascade lasers (QCLs) has been developed. A semi-classical transport model based on the Pauli master equation (PME) has been adopted as it is considered a good trade-off between physical accuracy and computational efficiency. The basis states for the PME are determined using a multi-band **k•p** Hamiltonian. In this way we account for non-parabolicity effects important to QCL modelling. The incoherent scattering processes included are due to acoustic and optical deformation potential interaction, polar optical phonons, alloy disorder and interface roughness. The master equation is solved using a Monte Carlo method. To provide a versatile research and engineering tool, the simulator has been optimized for efficiency and easy usability. A new algorithm has been developed that automatically distinguishes the field-periodic wave functions from the spurious states due to the artificial boundaries. We use quasi-bound states as basis functions, the life times of which allow us to estimate the coherent tunnelling current. The computation time for the polar-optical scattering rate has been reduced by more than three orders by a reformulation of the multiple integrations involved.. Output quantities of a transport simulation are current-voltage characteristics, the coherent current component, optical gain, incoherent lifetimes, subband populations and energy distributions. Several designs of MIR and THz QCL developed in P03 (Strasser) and P11 (Unterrainer) have been analysed, where good agreement of measured and simulated I-V curves was found.

The transport simulator has been integrated with the Vienna Schrödinger-Poisson Solver (VSP) which is used to compute the basis functions from a **k•p** Hamiltonian. Furthermore, the VSP has been extended to operate on two and three dimensional geometries. Unstructured meshes composed of triangular or tetrahedral elements are supported, which allow us to discretize complex device geometries. A common, dimensionality-independent discretization scheme has been introduced, which is flux conserving and properly deals with material anisotropy. The VSP has been used to characterize dielectric cavities. To model the radiative losses we assume perfectly matched layer boundary conditions which result in a non-hermitian eigenvalue problem. Since only a certain region of the cavity resonance spectrum is of practical interest, specific numerical methods for the solution of this inner eigenvalue problem are employed. An elliptic micro disk cavity has been used as a benchmark device for the optical mode calculation. The VSP has also been equipped with methods for electronic structure calculations for quantum dots. A **k•p** Hamiltonian for PbTe has been implemented and the electronic structure of PbTe quantum dots fabricated in P04 (Springholz) calculated.

#### 4.9.2 Scientific Background - State of the Art

The Vienna Schrödinger-Poisson solver (VSP) was the main tool for research used in this project phase (Karner 2007). The VSP simulation environment was successfully extended and used in several different physical contexts, including calculation of electronic structures, classical and semi-classical electron transport, as well as electromagnetic wave propagation and eigenmode calculation in optical devices. In order to address each of these contexts efficiently the VSP was designed to take the maximum advantage from the similarities existing between the particular physical problems, thus minimizing the model development time and maximizing the code reuse. In this section, we will briefly present the modelling framework of the VSP before describing the implemented models in detail.

##### The Vienna Schrödinger-Poisson Simulation Framework

A common simulation process is performed in three steps. First, the device geometry and mesh information are read from a file previously created by a graphical CAD (Computer Assisted Design) tool; they are processed and made available as data structures. Second, in the case of a deterministic problem, a system matrix is assembled based on the model equation; in this process step the local geometrical and topological information from the previous step is used to discretize the model equation. In the third step the system matrix is numerically processed (e.g. factorized, diagonalized) or a linear system is solved to obtain the simulation result. The three steps may be repeated to solve a nonlinear problem iteratively.

The VSP represents each of these process steps as a component of the simulation kernel. A so-called model entity controls the data flow between the three components by supplying the model equations, boundary conditions, and the problem type (linear system, eigenvalue, Green's function, and so forth). The geometry and topology component is supported by a number of reordering and decomposition algorithms for reducing simulation time and memory consumption (Davis 2006), while the numerics component calls various well-established state of the art numerical libraries and algorithms to perform the demanded numerical tasks. The physical models, the reordering and decomposition algorithms, and the numeric libraries each connect to the simulation kernel via a specific application programming interface (API).

##### Discretization and Numerics

The VSP framework uses a finite volume discretization scheme relying on a formulation based on the conservation of fluxes in each of the finite volumes. In this way the weak formulation fundamental to the finite element method is avoided. The fluxes are treated in

their full vectorial form which allows the treatment of material anisotropy within the finite volume scheme (Stanojevic 2011). The discretization scheme uses lines, triangles, and tetrahedra as its primitive element types, thus allowing the simulation of realistic one, two, and three-dimensional structures. The discretization formalism is dimensionality-independent; the input device geometry defines the dimensionality and even different dimensionalities can be mixed within one device, such as, for instance, three-dimensional electrostatics with two-dimensional carrier transport.

The computationally most challenging matrix-numerical problems encountered in the project were related to eigenpair calculations. On the one hand, complex devices and structures often result in large sparse system matrices. The Implicitly Restarted Arnoldi Method (IRAM) (Lehoucq, section 7.6 in Bai 2000) is used which scales roughly linearly with the matrix size due to the sparsity property. On the other hand, however, physically large devices have a spectrum consisting of closely spaced eigenvalues; this causes convergence issues in iterative algorithms such as IRAM. This problem is solved using a spectral transform called shift-and-invert which dramatically improves convergence but requires a matrix factorization. The VSP numerics component seamlessly integrates both the IRAM and the factorization libraries facilitating their effective use.

## **Optical Models**

The main goal of optical modelling is the spectral analysis of dielectric cavities, i.e. the calculation of the resonant frequencies and the corresponding eigenmodes. Under the assumption of a harmonically oscillating field the Helmholtz equation can be derived from the Maxwell equations. The Helmholtz equation can be readily discretized and solved by the methods described in the previous sections. The correct modelling of light radiating from the optical cavity necessitates the use of open boundary conditions. The idea of using absorbing boundary conditions, so called perfectly matched layers (PML), has been adopted in our simulations. The use of PMLs was discussed and their validity (under certain conditions) was shown in (Streiff 2004).

The problem of cavity eigenmode calculation requires the solution of an algebraic eigenvalue problem. The latter is non-hermitian due to the use of absorbing boundary conditions which are not energy conserving. As a consequence the resonant frequencies are complex-valued, where the imaginary part of an eigenfrequency represents the radiative losses of the particular eigenmode. For practical applications, e.g. a lasing structure, only a certain region of the cavity resonance spectrum is relevant, which is usually determined by the frequency interval where optical gain is provided. In the context of the algebraic eigenvalue problem, these resonances correspond to inner eigenvalues; these eigenvalues are inaccessible by simple vector and subspace iteration methods, and the structure size (tens of thousands of

points) prohibits the use of direct methods. Here, the shift-and-invert spectral transform discussed above allows for efficient calculation of the required portion of the cavity spectrum. The necessary factorization is carried out using a direct sparse solver (Demmel 1999) combined with a fast geometry-based nested dissection reordering scheme, resulting in a computational times and memory consumption close to the theoretical limit for two-dimensional geometries (Davis 2006).

### **Electronic structure models**

One important class of problems is the determination of the electronic structure in nanostructures exhibiting geometrical and electrostatic confinement. These structures include epitaxially grown heterostructures such as quantum wells or quantum cascade laser (QCL) structures, ultra-thin films, nanowires, and quantum dots. The essence of the problem is the solution of the Schrödinger equation in one, two, or three dimensions. The Hamiltonians used are derived from **k**•**p** theory and take into account up to eight bands. At present only cubic semiconductors are considered, such as Si and SiGe, group III-V compound semiconductors (implemented in project phase 1) and leadsalts such as PbTe (implemented in project phase 2). The spatial discretization of the **k**•**p** Hamiltonians poses several problems. One is anisotropy, which is not only present in the valleys of the bands themselves, but also in the couplings between the bands, which contribute non-diagonal terms of the form  $k_x \cdot k_y$ . This problem has been effectively solved by the finite volume discretization mentioned previously. Another difficulty arises from the first order contributions in the Hamiltonian. These terms adversely affect the numerical stability of the discretization and special care has to be taken to prevent oscillatory results in the eigenstates.

### **Transport model for Quantum Cascade Lasers**

The characteristics of a QCL are mainly determined by the designer's choice of material and quantum well geometry. For this purpose, simulation tools are very useful to help the designer achieve the desired optical and electrical characteristics and to optimize the QCL design. A requirement for such a simulator as a Technology CAD (TCAD) tool is a good balance between computational speed and physical accuracy. To describe cross-plane transport in a QCL hetero-structure the usage of basically three quantum transport models has been reported in literature. The non-equilibrium Green's function formalism (NEGF) represents the most rigorous approach (Kubis 2007, Lee 2002). However, the inherently high computational costs of the NEGF formalism render it unfeasible as a TCAD tool. The density matrix approach is capable of handling coherent phenomena in addition to dissipative scattering processes (Callebaut 2005). One shortcoming of this approach is that scattering is often treated by a simple relaxation time approximation. In this way the rich physics included

in the scattering self-energies of the NEGF approach and in the scattering operator of the semi-classical approach is neglected. Theoretical studies showed that in many practical cases the steady state transport in QCLs is incoherent and therefore, a semi-classical description is applicable (Iotti 2001, Jirauschek 2007). The semi-classical transport equation follows from the Liouville-von Neumann equation after applying the Markov approximation to the fully non-diagonal density matrix formulation (Iotti 2005) and introducing the diagonal approximation. The result is a set of coupled Boltzmann-like equations, also known as the Pauli master equation (Fischetti 1999), where the transition rates are given by Fermi's Golden Rule. Based on the semi-classical approach we developed a transport simulator for QCLs, which solves the Pauli master equation numerically (Milovanovic 2011, Baumgartner 2011). Transport is described via in-scattering to and out-scattering from stationary states. The deep understanding of the semi-classical approach gained in this project phase allows us to propose in the third project phase an extended approach that will include coherent tunnelling as well.

Because of the periodic structure of a QCL it is sufficient to simulate the electron transport through one central stage only. The wave function overlap between the central stage and the spatially remote stages is small such that one can assume inter-stage scattering to be limited to the next nearest neighbours. The electronic basis states corresponding to a single QCL stage are evaluated from a self-consistent Schrödinger-Poisson solution. Only field-periodic wave functions are retained, whereas spurious states due to the artificial boundaries in the simulation are discarded. The electronic states in the multi quantum well structure are replicas of the states in the central stage. In a similar way, field-periodic boundary conditions can be imposed on the Pauli master equation. The carrier transport is simulated over the central stage and every time a carrier undergoes an inter-stage scattering process, the electron is reinjected into the central region with an energy changed by the voltage drop per period, and the corresponding electron charge contributes to the current.

The transport equation can be either solved by direct discretization or a Monte Carlo method. We have chosen the latter and devised several new numerical methods to reduce computation time (Baumgartner 2011).

### **4.9.3 Results and Discussion**

#### **Spectral analysis of dielectric cavities**

A VSP model has been developed which calculates the eigenmodes of dielectric structures. The model uses the perfectly matched layer (PML) absorbing boundary conditions to emulate an open simulation domain, allowing light to escape from the cavity. This allows the

correct modelling of radiative losses of the cavity, which are quantitatively obtained from the imaginary part of the complex eigenfrequencies.

Motivated by the microdisc lasers fabricated in project P04 (Springholz) we have chosen a two-dimensional elliptical microdisc cavity as a benchmark device. The elliptical shape of the resonator does not allow the modes to be calculated by separation in radial and azimuthal modes. This necessitates a full numerical approach. The simulation domain consists of three regions: the microdisc, i.e. the actual cavity, the propagation medium, essentially a buffer with unity refractive index, and the PML.

The calculation of the cavity eigenfrequencies and eigenmodes requires the solution of a non-hermitian algebraic eigenvalue problem. Furthermore, only eigenvalues with a small imaginary part are of interest since solutions with larger imaginary parts are not confined to the cavity and therefore are not relevant for the lasing operation. To obtain the desired modes the shift-and-invert spectral transformation is used (Lehoucq in Bai 2000). The poles of the spectral transform are placed along the real axis. A subspace iteration (IRAM) is then performed, looking for the largest transformed eigenvalues, i.e. closest to the pole, which converges after only a few iteration steps. This allows calculating only a selected few eigenfrequencies and eigenmodes, which are physically meaningful and relevant to the application. The spectral transform itself is computed using the SuperLU direct sparse solver (Demmel 1999), which ensures high accuracy while keeping time and memory requirements at a moderate level.

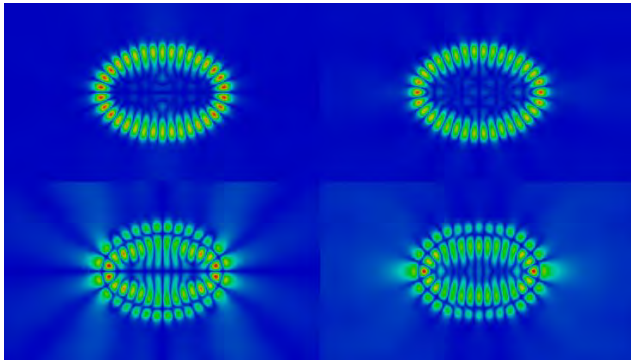


**Figure 1:** Four confined modes of the elliptical resonator

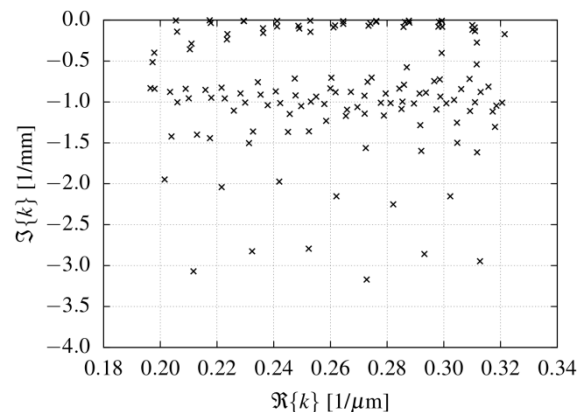


**Figure 2:** Eigenfrequencies of the microdisc. The stable modes are located close to the real axis

Fig. 2 shows the calculated part of the cavity resonance spectrum. The states confined to the cavity can be seen clustered close to the real axis (top of the figure). The remainder of the eigenfrequencies are not physical because they are confined within the propagation medium, an effect which arises from the finite simulation domain; they are a necessary by-product of

the subspace iteration algorithm (IRAM). Four of the confined or "stable" modes of the elliptical resonator are depicted in Figure 1.

To evaluate the performance and scalability of the calculation, the elliptical cavity problem was analyzed several times varying the mesh size from a few ten thousand points up to half a million. A roughly linear dependence of simulation time and memory consumption was found, which indicates that simulations up to one million points are feasible on a contemporary workstation computer, allowing the simulation of large and complex cavity structures.

### Electronic Structure of Quantum Dots

As a general purpose partial differential equation solver the VSP can be employed in electronic structure calculations as well. The  $\mathbf{k}\cdot\mathbf{p}$  Hamiltonian described in (Kriechbaum 1984) has been implemented. First results for a PbTe quantum dot are shown in Figure 3. A more detailed analysis of the optical transitions and the validation against photoluminescence measurements from P04 (Springholz) is currently conducted and will extend into the next project phase. In this way we are complementing the activities in P13 (Vogl) by considering materials not available in nextnano.

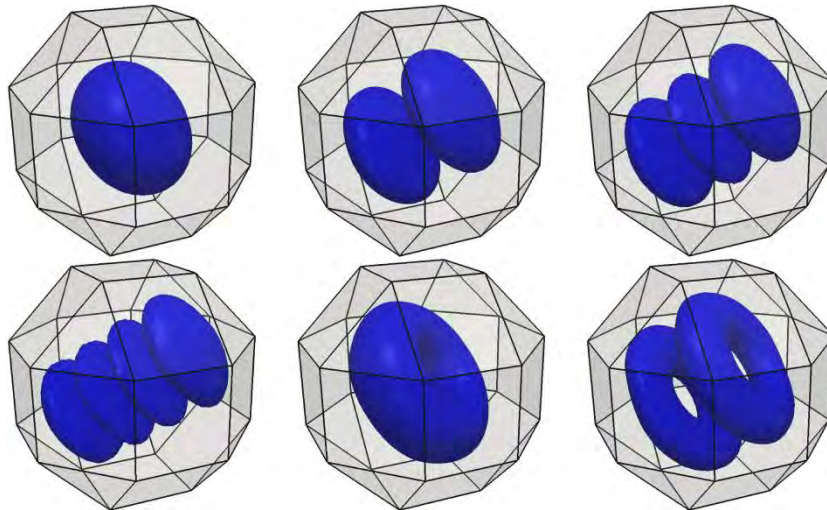


**Figure 3:** Electron densities for the first six eigenstates in a 5 nm wide PbTe quantum dot

Since no experimental data for nanowire optoelectronic devices became available in this project phase we have deviated from the original workplan. This SFB gives us the unique opportunity to develop our theoretical models in accordance with the needs and the results of the experimental partners. If this experimental basis is missing for a particular nanostructure we considered it justified to redirect our focus to structures more relevant to this SFB, such as the leadsalt quantum dots. Nevertheless, outside this SFB we conducted considerable research on electronic structure and transport in nanowires using both tight binding

(Neophytou 2010, 2010b, 2011 ) and **k•p** methods (Stanojevic 2010, Baumgartner 2010). Thus we have the methods and tools for nanowire devices available for the next project phase if needed.

### **Efficient Monte Carlo Simulator for Quantum Cascade Lasers**

The task at hand can be separated into two parts. First the basis states need to be determined for which the VSP was used. Since it is essential to consider band non-parabolicity for QCLs the user can choose one of several models for the Hamiltonian of the system. An effective two-band **k•p** model (Sirtori 1994) or a three-band **k•p** model are available in addition to a single-band, effective mass model. Usage of the available eight-band **k•p** model can in many cases be avoided, since it reduces to the three-band **k•p** model for vanishing in-plane momentum.

To describe the openness of the quantum system we assume perfectly matched layer (PML) boundary conditions for the Schrödinger equation (Odermatt 2005). These boundary conditions give rise to a non-Hermitian eigenvalue problem which is solved by means of Arnoldi iteration and the ARPACK library linked to VSP. In this way we obtain complex eigenvalues, the imaginary part of which determines the finite lifetime due to coherent tunnelling. Using quasi-bound states as a basis for the master equation allows us to estimate the coherent tunnelling component of the current from the states' lifetimes and occupations (Karner 2006). The semi-classical approach will break down if the coherent current component becomes comparable to the incoherent current component due to scattering, a criterion that can now be checked in our simulations.

We investigated a InGaAs/GaAsSb mid-infrared QCL developed in project P03 (Nobile 2009). The wave functions for PML boundary conditions are shown in Figure 4. Restricting the calculation to a finite number of stages, for example, three in our case, will cause the occurrence of spurious states. These are induced by the artificial boundaries and would not be present in a field-periodic cascade. We developed a method to select the field-periodic states automatically. For this purpose we calculate the cross-correlation and auto-correlation of all wave functions using the Fast Fourier Transform (FFT). If the position of the maximum of a cross-correlation function is equal to the period length of the QCL structure, the two states are considered periodic and given an appropriate stage index. The result of the automatic selection of the periodic states is shown in Figure 4.

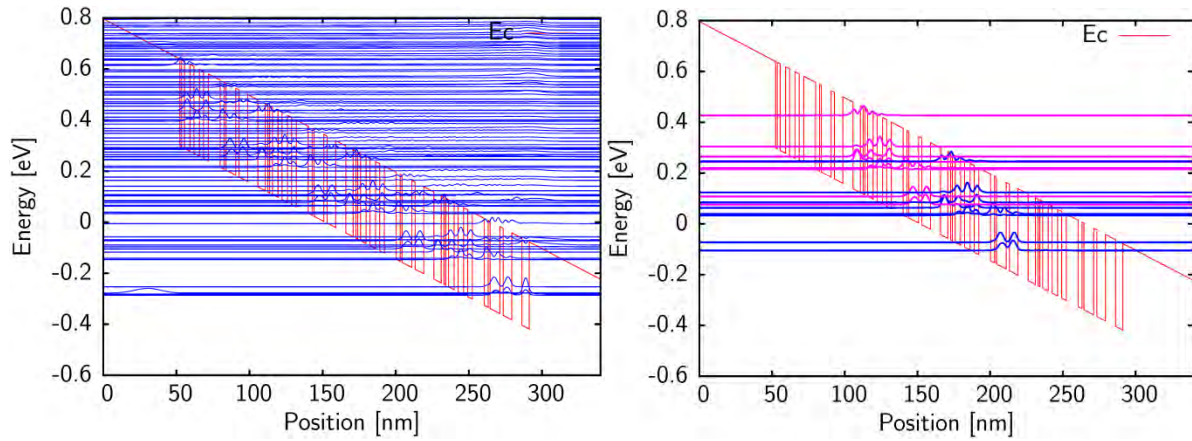


**Figure 4:** Left: Multiple cascades of a QCL need to be considered to obtain realistic basis states for the PME. Right: Application of our subband selection routine automatically assigns the periodic wavefunctions to a stage of the QCL (only the states of two stages are shown)

The second part is the Monte Carlo (MC) routine to solve the Pauli master equation. Currently, acoustic and optical deformation potential, and polar optical electron-phonon scattering as well as inter-valley, alloy, and interface roughness scattering are available in the model. The object oriented implementation allows simple inclusion of additional scattering mechanisms. In the next project phase we shall add binary electron-electron scattering and the electron-photon interaction.

We identified the calculation of the scattering rate by polar-optical phonons as one of the most time consuming steps. Therefore, we optimized the calculation of the scattering rate for this process by exchanging the order of the multiple integrations involved. Integration over the final states is carried out first, which can be done analytically, whereas an integration related to the matrix element is carried out last. The remaining integration is in momentum space and has the form (Milovanovic 2010)

$$\Gamma_{mn}(\mathbf{k}_{\parallel}) = \frac{m}{\hbar^2} \frac{e^2 \omega_{\text{PO}}}{4\pi\epsilon} \left( n_{\text{PO}} + \frac{1}{2} \mp \frac{1}{2} \right) \int \frac{|\hat{\rho}_{mn}(q_z)|^2}{\sqrt{(k_{\parallel}^2 + k_f^2 + q_z^2)^2 - 4k_{\parallel}^2 k_f^2}} dq_z$$

The overlap integrals  $\hat{\rho}_{mn}(q_z) = \mathcal{F}\{\rho_{mn}(z)\}$  where  $\rho_{mn}(z) = \psi_m^* \psi_n$  are calculated efficiently using the FFT. This approach reduces the calculation time of the PO scattering rate by three to four orders of magnitude as compared to a numerical evaluation of the standard textbook formula.

The energy dependence of all scattering rates is precalculated and stored in tables. In the MC main loop only a fast look-up and selection according to the pre-calculated scattering rates is necessary. The current state and the chosen scattering process are then used to update the statistical quantities such as subband population, energy distribution, and current. We applied the implemented model to the MIR QCL structure of Figure 4 and calculated the electric field vs. current density characteristics at 78K as shown in Figure 5. The simulation

result is in good agreement with the experiment up to the laser threshold. Above 32.5 kV/cm the results of the semi-classical model lose validity as the coherent tunnelling current starts to increase rapidly. The characteristics show that the X valley contributes only marginally to the total current near the laser threshold. This is also indicated by the scattering rates for the lower laser level depicted in Figure 6 which identify PO emission as dominant process for that subband.

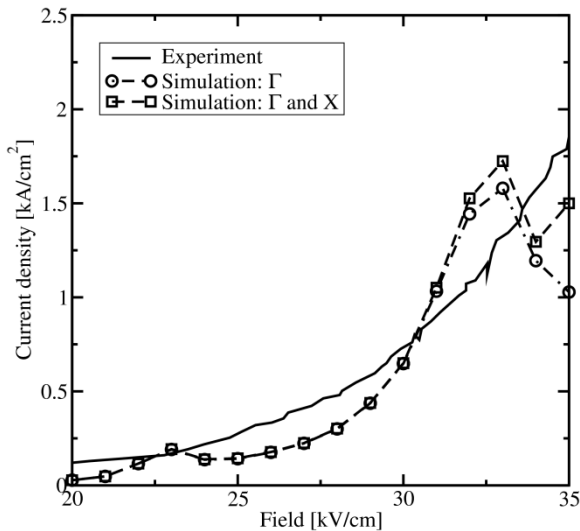


**Figure 5:** Current density vs. applied electric field of the MIR QCL. The simulation shows that the inclusion of the X valley has no considerable influence on the characteristics around the laser threshold of 30 kV/cm

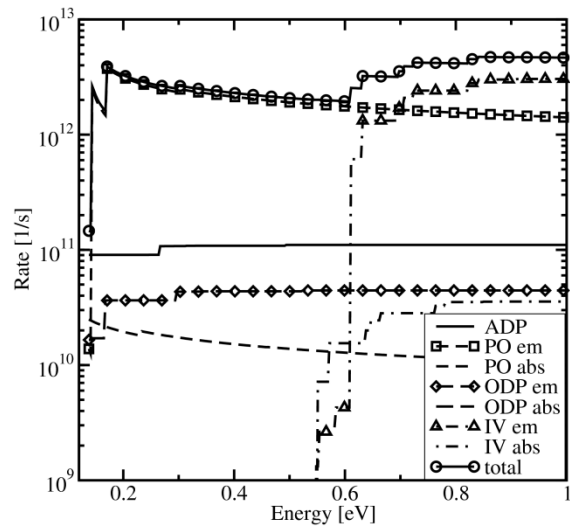


**Figure 6:** Calculated scattering rates of the lower laser level. At energies near the subband minimum the polar optical emission is the dominant process. This ensures fast depopulation of the lower laser level

The calculation of a single operating point typically takes a few minutes, depending on number of valleys, subbands and energy grid resolution. This is orders of magnitude faster than a full quantum treatment with non-equilibrium Green's functions, but still gives insight to microscopic quantities such as the carrier density spectrum shown in Figure 7.

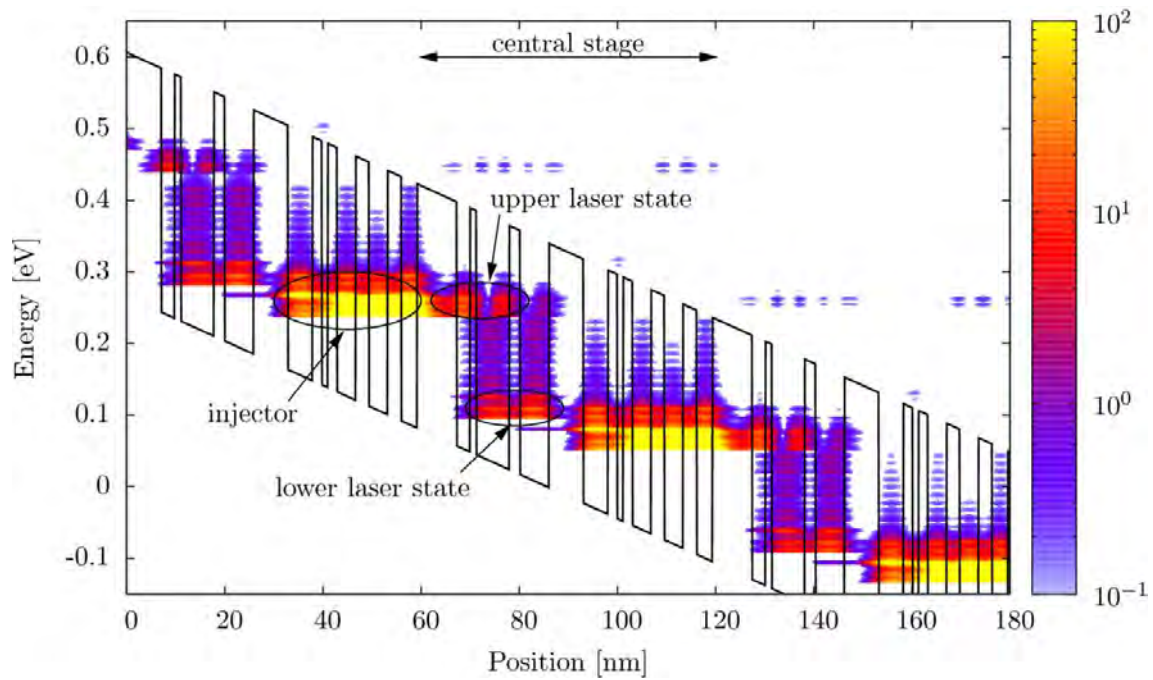


**Figure 7:** Conduction band edge and carrier density spectrum obtained by the Pauli master equation solver at an electric field strength of 30 kV/cm. The occupation of the upper laser state is clearly visible

#### 4.9.4 Collaboration within and beyond the SFB

Development of new QCL designs and concepts is one of the main research areas in this SFB. The non-equilibrium Green's function (NEGF) method will give the most rigorous description of transport in these devices, but is known for the huge computation times required, especially if incoherent scattering and more complex structures must be considered. In P13 (P. Vogl) computation times for an I-V curve in excess of one week are reported. For this reason we pursued the semi-classical approach from the very beginning, whereas in P13 approximations to the NEGF method were sought to reduce the computational burden. In the development phase of the semi-classical QCL simulator, which took the bigger part of this project phase, we used the MIR and THz designs from P03 (Strasser) and P11 (Unterrainer) for case studies and model validation (Milovanovic 2010, Milovanovic 2011). With these project partners located at the same University we have regular meetings to address specific issues of QCL design, such as temperature effects, interface roughness, and hot carriers, to name a few. The code has been transferred to these partners and students trained.

The multi-dimensional finite-volume simulator VSP was enhanced and used to characterize microdisc optical cavities and to calculate the electronic structure of lead salt quantum dots. This initiates collaboration with P04 (Springholz), which we shall intensify in the next project phase.

We established an external collaboration with Gerhard Klimeck from Purdue University on electronic structure and transport in nanowires (Neophytou 2010). In our group we have developed both tight-binding and **k•p** codes for calculating the electronic structure of nanowires, which are available in the next project phase if needed.

#### 4.9.5 References

Baumgartner O., Z. Stanojevic, G. Milovanovic and H. Kosina (2011), Efficient Simulation of Quantum Cascade Lasers using the Pauli Master Equation, Simulation of Semiconductor Processes and Devices, SISPAD 2011, in print (Sep. 2011)

O. Baumgartner, M. Karner, V. Sverdlov, H. Kosina (2010), Electron Subband Structure in Strained Silicon UTB Films from the Hensel-Hasegawa-Nakayama Model - Part 2 Efficient Self-Consistent Numerical Solution of the k.p Schrödinger Equation, Solid-State Electronics 54, 143, [DOI: 10.1016/j.sse.2009.12.010](https://doi.org/10.1016/j.sse.2009.12.010)

Bai Z., J. Demmel, J. Dongarra, A. Ruhe and H. van der Vorst (ed.) (2000), Templates for the solution of algebraic eigenvalue problems: a practical guide, [online available](#)

Callebaut H. and H. Qing (2005), Importance of coherence for electron transport in terahertz quantum cascade lasers, Journal of Applied Physics, 98, 104505, [DOI: 10.1063/1.2136420](https://doi.org/10.1063/1.2136420)

Davis T. A. (2006), Direct Methods for Sparse Linear Systems, SIAM

Demmel J. W., S. C. Eisenstat, J. R. Gilbert, X. S. Li and J. W. H. Liu (1999), A supernodal approach to sparse partial pivoting, SIAM J. Matrix Analysis and App. 20, 720-755, [DOI: S0895479895291765](https://doi.org/S0895479895291765)

Fischetti M. V. (1999), Master-equation approach to the study of electronic transport in small semiconductor devices, Phys. Rev. B, 59, 4901, [DOI: 10.1103/PhysRevB.59.4901](https://doi.org/10.1103/PhysRevB.59.4901)

Iotti R. C. and F. Rossi (2001), Nature of Charge Transport in Quantum-Cascade Lasers, Phys. Rev. Lett. 87, 146603, [DOI: 10.1103/PhysRevLett.87.146603](https://doi.org/10.1103/PhysRevLett.87.146603)

Iotti R. C., E. Ciancio and F. Rossi (2005), Quantum transport theory for semiconductor nanostructures: A density-matrix formulation, Phys. Rev. B 72, 125347, [DOI: 10.1103/PhysRevB.72.125347](https://doi.org/10.1103/PhysRevB.72.125347)

Jirauschek C., G. Scarpa, P. Lugli, M.S. Vitiello and G. Scamarcio (2007), Comparative analysis of resonant phonon THz quantum cascade lasers, Journal of Applied Physics 101, 086109, [DOI: 10.1063/1.2719683](https://doi.org/10.1063/1.2719683)

Karner M., A. Gehring, H. Kosina (2006), Efficient Calculation of Lifetime Based Direct Tunneling Through Stacked Dielectrics, Journal of Computational Electronics 5, 161, [DOI: 10.1007/s10825-006-8837-y](https://doi.org/10.1007/s10825-006-8837-y)

Karner M., A. Gehring, S. Holzer, M. Pourfath, M. Wagner, W. Gös, M. Vasicek, O. Baumgartner, Ch. Kernstock, K. Schnass, G. Zeiler, T. Grasser, H. Kosina, S. Selberherr (2007), A Multi-Purpose Schrödinger-Poisson Solver for TCAD Applications, Journal of Computational Electronics 6, 179, [DOI: 10.1007/s10825-006-0077-7](https://doi.org/10.1007/s10825-006-0077-7)

Kriechbaum M., K. E. Ambrosch, E. J. Fantner, H. Clemens, and G. Bauer (1984), Electronic structure of PbTe/Pb<sub>1-x</sub>Sn<sub>x</sub>Te superlattices, Phys. Rev. B. 30, 3394, [DOI: 10.1002/pssb.2221380126](https://doi.org/10.1002/pssb.2221380126)

Kubis T. and P. Vogl (2007), Self-consistent quantum transport theory: Applications and assessment of approximate models, J. Comput. Electron. 6, 183-186, [DOI: 10.1007/s10825-006-0078-6](https://doi.org/10.1007/s10825-006-0078-6)

Lee S.-C. and A. Wacker (2002), Nonequilibrium Green's function theory for transport and gain properties of quantum cascade structures, Phys. Rev. B 66, 245314, [DOI: 10.1103/PhysRevB.66.245314](https://doi.org/10.1103/PhysRevB.66.245314)

Milovanovic G., H. Kosina (2010), A Semiclassical Transport Model for Quantum Cascade Lasers based on the Pauli Master Equation, Journal of Computational Electronics 9, 3-4; 211, [DOI: 10.1007/s10825-010-0325-8](https://doi.org/10.1007/s10825-010-0325-8)

Milovanovic, G. (2011), Numerical Modeling of Quantum Cascade Lasers, PhD Thesis, TU Wien

Neophytou N., H. Kosina (2011), Effects of Confinement and Orientation on the Thermoelectric Power Factor of Silicon Nanowires, Physical Review B 83, 245305-1, [DOI: 10.1103/PhysRevB.83.245305](https://doi.org/10.1103/PhysRevB.83.245305)

Neophytou N., S. Kim, G. Klimeck and H. Kosina (2010), On the Bandstructure Velocity and Ballistic Current of Ultra-Narrow Silicon Nanowire Transistors as a Function of Cross Section Size, Orientation, and Bias, Journal of Applied Physics 107, 113701, [DOI: 10.1063/1.3372764](https://doi.org/10.1063/1.3372764)

Neophytou N., H. Kosina (2010b), Large Enhancement in Hole Velocity and Mobility in p-type [110] and [111] Silicon Nanowires by Cross Section Scaling: An Atomistic Analysis, Nano Letters 10, 4913, [DOI: 10.1021/nl102875k](https://doi.org/10.1021/nl102875k)

Nobile M., et al. (2009), Quantum cascade laser utilising aluminium-free material system: InGaAs/GaAsSb latticematched to InP, Electron. Lett. 45, 20, 1033, [DOI: 10.1049/el.2009.1995](https://doi.org/10.1049/el.2009.1995)

Odermatt S., M. Luisier and B. Witzigmann (2005), Bandstructure calculation using the  $k \cdot p$  method for arbitrary potentials with open boundary conditions, J. Appl. Phys. 97, 046104, [DOI: 10.1063/1.1847695](https://doi.org/10.1063/1.1847695)

Sirtori C., F. Capasso, J. Faist and S. Scandolo (1994), Nonparabolicity and a sum rule associated with bound-to-bound and bound-to-continuum intersubband transitions in quantum wells, Phys. Rev. B 50, 8663, [DOI: 10.1103/PhysRevB.50.8663](https://doi.org/10.1103/PhysRevB.50.8663)

Stanojevic Z., O. Baumgartner, V. Sverdlov, H. Kosina (2010), Electronic Band Structure Modeling in Strained Si-Nanowires: Two Band  $k \cdot p$  Versus Tight Binding; in: Proceedings of the 14th International Workshop on Computational Electronics (IWCE), ISBN: 978-1-4244-9381-4; 5-8

Stanojevic Z., M. Karner, K. Schnass, C. Kernstock, O. Baumgartner and H. Kosina (2011), A Versatile Finite Volume Simulator for the Analysis of Electronic Properties of Nanostructures, Simulation of Semiconductor Processes and Devices, SISPAD 2011, in print (Sep. 2011)

Streff, M. (2004), Opto-Electro-Thermal VCSEL Device Simulation, PhD Thesis, ETH Zürich, [DOI: 10.3929/ethz-a-004711416](https://doi.org/10.3929/ethz-a-004711416)

***For a complete list of publications of this project part please refer to p. 59 (2.1 List of publications)!***